

# Distribution of $^{137}\text{Cs}$ and $^{210}\text{Pb}$ in sediments of tidal flats in north Jiangsu Province

LIU Zhiyong, \*PAN Shaoming, LIU Xuying, GAO Jianhua

Ministry of Education Key laboratory of Coastal and Island Development, Nanjing University, Nanjing 210093, China

**Abstract:** Seven cores were collected from different sediment zones of tidal flats at Xinyanggang in north Jiangsu province in August 2007. Sediment grain-size distribution and radioisotopes of  $^{137}\text{Cs}$  and  $^{210}\text{Pb}$  analysis were carried out for these cores. Sediment rates of the cores and radioisotopes distribution in surface sediment in different zones of the tidal flat were calculated from the  $^{137}\text{Cs}$  and  $^{210}\text{Pb}$  activities in sediments cores. The results indicated that each tidal zone had experienced different evolution phases, hydrological dynamics in the tidal flats made the grain-size of the surface sediment change gradually.  $^{137}\text{Cs}$  and  $^{210}\text{Pb}$  activities on the superficial layer of the cores varied spatially and the reason was discussed. On tidal flats, the fluctuation of  $^{137}\text{Cs}$  and  $^{210}\text{Pb}$  activities in the cores reflected the special sedimentary characteristics. Vegetation affects the grain-size distribution and the vertical profiles of  $^{137}\text{Cs}$  and  $^{210}\text{Pb}$  in the upper depths.  $^{137}\text{Cs}$  and  $^{210}\text{Pb}$  chronology got the comparable average sediment rates on the tidal flat. The characteristics of  $^{137}\text{Cs}$  and  $^{210}\text{Pb}$  in the cores reflected various depositional dynamical environments in different tidal zones and gave information on the different evolvement phases of the tidal zones. Based on the information of grain-size distribution, texture of the cores, sediment rates and topography, the evolution lines of the tidal flat were reconstructed.

**Keywords:** tidal flats; grain-size information;  $^{137}\text{Cs}$  and  $^{210}\text{Pb}$  dating; sediment rates; north Jiangsu province

## 1 Introduction

The tidal flats in north Jiangsu province is one of the typical muddy/silty coasts in China. As the largest continuously distributed coastal wetland in terms of area coverage (5100 km<sup>2</sup>) in China (Wang and Zhu, 1990), the wetland plays an important role in the landward deposition of abundant fine-grained sediment from the Yellow Sea and has global ecological and biodiversity protection significance. The tidal flats in Jiangsu Province extend 884 km long from north to south, with an average width from 10 km to 13 km. Because of the variation of sediment sources, the erosion or deposition coastal line is not constant in history (Wu and

**Received:** 2008-10-29 **Accepted:** 2009-05-06

**Foundation:** National Basic Research Program of China, No.2002CB412401; Scientific Research Foundation of Graduate School of Nanjing University; National Natural Science Foundation of China, No.40776023

**Author:** Liu Zhiyong (1981–), Ph.D Candidate, specialized in coastal environment. E-mail: yongjxu@163.com

\***Corresponding author:** Pan Shaoming, E-mail: Span@nju.edu.cn

Wang, 2005). Sediments from the old Yellow River and the Changjiang River estuaries, are two dominating sediment sources. They accumulate into the middle part of Jiangsu coast and aggrandize the coast in the total area and strengthen the dimension and height of the radiative sand ridges (Chen, 1991).

The tidal flats have subjected to intensive anthropogenic influence because of reclamation and dredge. Artificial introduction of *Spartina angilica* and *Spartina alterniflora* exert a great influence on the bed accretion, changing the evolution process of the tidal flat morphology (Wang *et al.*, 2006). Sediment processing is a vital element to maintain the ecosystem of the intertidal zone, and the geomorphologic evolution greatly relates to the structure and function of the tidal ecosystem. Sediment grain-size has recorded the historic information on hydrodynamic conditions, sediment sources, sediment processing and vegetations on the tidal flats (Wang *et al.*, 2004; Li *et al.*, 2007).

Modern sediment is a key indicator of geomorphologic evolution (Xia *et al.*, 2004), and sedimentary records contain information on ancient environmental changes, which is obtained by analyzing bore holes or cores through the grain-size distribution, the age of the sedimentary material and sedimentary structures (Gao, 2009). Radioactively isotopes such as  $^{137}\text{Cs}$  and  $^{210}\text{Pb}$  have been thoroughly researched and widely used as a tracer to evaluate the sedimentary processes in oceans, rivers and lakes (Wan, 1995; David and Steven, 1995; Guebuem *et al.*, 1997). Moreover, the sediment profiles of  $^{137}\text{Cs}$  and  $^{210}\text{Pb}$  make insight into the modern sediment process (Pan, 1997; Perianez, 2008). Anthropogenic radionuclide  $^{137}\text{Cs}$  is the result of nuclear power testing, with a half-life as 30.2 y, as soon as atmospheric deposition to the land, attached to the fine-grained sediment and transport within it. In coastal area, major source of  $^{137}\text{Cs}$  is coming from atmospheric deposition and vertical  $^{137}\text{Cs}$  profile of sediment core relates to the temporal series fallout of the  $^{137}\text{Cs}$  in global area (Pennington, 1973; Pan *et al.*, 2008). Variations in  $^{137}\text{Cs}$  concentration with depth of sediment core can therefore be compared with the fallout record through time (Goff, 1997). The year of first significant  $^{137}\text{Cs}$  fallout was 1953, while 1963 was the year of maximum global cesium fallout. Nuclear weapon test after the 1970s made another detectable level in some parts of the world, especially in the Northern Hemisphere (Zhang *et al.*, 2005). Regional nuclear accident like the Chernobyl in 1986 made big fallout of  $^{137}\text{Cs}$ . These accumulating inventories can be used as indicator to dating.  $^{210}\text{Pb}$  is a naturally occurring radioactive isotope, the activity of  $^{210}\text{Pb}$  (half-life of 22.3 y) in sediment contains two parts. The first part coming from uranium decay series of  $^{226}\text{Ra}$  within the sediment (supported  $^{210}\text{Pb}$ , marked as  $^{210}\text{Pb}_{\text{com}}$ ), another part coming from atmospheric scavenging processes (e.g. rain, snow, dry fallout, etc.) which originated from thorium decay series of  $^{222}\text{Rn}$  (unsupported or exceeded  $^{210}\text{Pb}$ , marked as  $^{210}\text{Pb}_{\text{ex}}$ ) (Nriagu, 1978).

Dating profiles from intertidal areas are more difficult than supra tidal marshes or subtidal marine sediments that have generally given more consistent results, including the reworking caused by bioturbation and resuspension induced by currents and waves made problems to reckon the sediment rates (Thorbjorn *et al.*, 2000). Sediment rates in the tidal flats of Jiangsu have been reported based on topography (Zhu *et al.*, 1986; Yang, 2002) or isotopes, and the influence on sediment rates caused by vegetation as *Spartina* were estimated (Wang *et al.*, 2006; Gao *et al.*, 2007). However, there have been very few studies on the evolution or zonation characteristic of the tidal flats based on sediment grain-size and isotopes in the last

few decades. In order to make a full view of the evolution of the tidal flats, the objectives of the present study are to: (1) analyze the sediment grain-size distribution information on the different zones of the tidal flat, (2) detect the distribution characteristic of  $^{137}\text{Cs}$  and  $^{210}\text{Pb}$  in sediments cores, and (3) evaluate the sediment rate and the evolution processing of the tidal flat. The findings will be useful in better understanding the structures and functions in different zones of the tidal flat and promoting the development and protection of the valuable wetland resource.

## 2 Study area

Xinyanggang is situated in the core area of the National Nature Reserve in Yancheng, which is a typical tidal ecosystem, almost an intact tidal flat in Jiangsu Province. The surface distribution from sea toward land is the silt-fine sand and mud-sand mixed tidal flat, the *Spartina angilica*–*Spartina alterniflora* tidal flat, the *Suaeda salsa* tidal flat, and the *Phragmites australis* tidal flat, 4 parallel zones (Wang and Zhu, 1990; Gao *et al.*, 1997) (Figure 1). With abundant sediment supply transporting from sea to land unceasingly, the four parallel zones extend seaward year by year (Ke, 1993). The tidal flat at Xinyanggang carries large

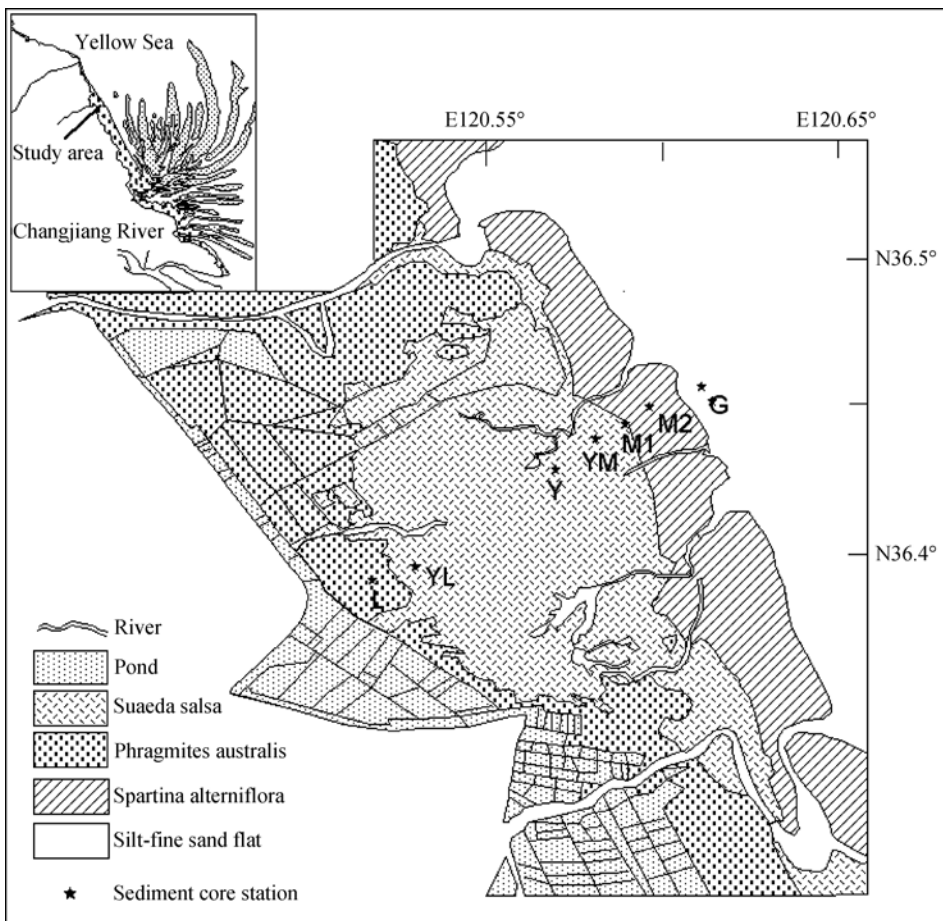


**Figure 1** Location of the study area and sampling sites

amounts of fine-grained suspended sediments and is approximately 10 km wide. The average slope of the tidal flat is  $0.55 \times 10^{-3}$  and the average tidal range is 3.68 m. Because the area is separated from the nearest offshore tidal ridge by open waters of 20 km in distance, its environment has a high degree of openness in terms of hydrodynamics (Wang *et al.*, 2006). The annual mean temperature is  $14.4^\circ\text{C}$  and annual mean precipitation is 1020 mm. The tidal flat is affected by the marine monsoon climate with prevailing southeastern wind in summer and prevailing northwestern wind controlled by tropical depression in winter (Ren, 1986).

### 3 Sampling and analysing

In August 2007, seven sediment cores were collected using a hand-driven PVC coring tube. Samples were taken from different zones of the tidal flat at intervals about 1 km from land to sea. Surface vegetation on the tidal flat was translated gradually from *Phragmites australis*, *Suaeda salsa* to *Spartina alterniflora*. These cores were ranged from 77 to 136 cm in depth. Sediment core at the *Phragmites australis* zone was marked as L, the *Phragmites australis* and *Suaeda salsa* transitional zone as YL, the *Suaeda salsa* zone as Y, the *Suaeda salsa* and *Spartina alterniflora* transitional zone as YM, the *Spartina alterniflora* zone as M, and the silt-fine sand and mud-sand mixed zone as G. After they were taken into the laboratory, these sediment cores were sliced open, described for stratigraphy and cut into 2 cm thick slice for further analysis. For all the sediment cores, a separate sample aliquot of 2 g sediment was pretreated using 15 ml of 0.6%  $(\text{NaPO}_3)_6$  for 24 h for being dispersed and homogenized. The grain-size of the cores was determined by a laser particle analyzer (Master 2000, Product of Malvern Instruments, the UK), and grain-size parameters were calculated by the Moment method (Mcmanus, 1988). Other samples were weighed and dried at  $80^\circ\text{C}$  for 6 days. Water contents were determined by weight loss after drying. The dried samples were ground, sealed in plastic bins more than 21 days for the equilibrium to occur between  $^{226}\text{Ra}$  and  $^{222}\text{Rn}$  (Chanton, 1983).

$^{137}\text{Cs}$  peaks were corresponded to the years as described before. Dating of the sediment cores by  $^{137}\text{Cs}$  is based on the recognition of some or all of the detectable peaks in the sedimentary records (Thorbjorn *et al.*, 2000).

Assuming constant  $^{210}\text{Pb}_{\text{ex}}$  flux, a sedimentation rate at a given depth can be estimated by attributing a decrease in  $^{210}\text{Pb}_{\text{ex}}$  in the deep profile to the radioisotope decay and this method is CRS (Constant Rate of Supply) model (Shigeru *et al.*, 2006). The calculation of ages is determined as follows:

$$T = (1/\lambda) \ln(I_z / I_{\text{tot}}) \quad (1)$$

where  $T$  is the age,  $I_z$  the inventory of  $^{210}\text{Pb}_{\text{ex}}$  at depth of  $Z$ ,  $I_{\text{tot}}$  the total inventory of  $^{210}\text{Pb}_{\text{ex}}$  in the core section and  $\lambda$  is the constant of decay of the  $^{210}\text{Pb}$  (Adam *et al.*, 2008).

To test the  $^{137}\text{Cs}$  and  $^{210}\text{Pb}$  activities, Germanium ray spectrometry made by ORTEC in the US (GMX30P-A) was used in the Ministry of Education Key Laboratory of Coastal and Island Development in Nanjing University. The gamma activity of each sediment sample was measured for 72,000 s. Reference sample was supplied by the Bedford Institute of Oceanography in Canada (65.4 g, 806.2 Bq/kg, 72000 s).

## 4 Results and discussion

### 4.1 The characteristics of grain-size distribution

#### 4.1.1 Profiles of mean grain-size and components

The grain-size distribution characteristics of the sediment profiles are presented in Figure 2. G, gray, is mainly composed of sand. The mean grain-size varies from  $3.92\Phi$  (0–77 cm) to  $3.48\Phi$  (>77 cm).  $M_2$ , the color and the mean grain-size are obviously distinct near 65 cm in the sediment profile, residual *Spartina* roots are found in the profile, mean grain-size is  $4.48\Phi$ , and sediment components is changing from 50% sand and 50% silt at the lower part to mostly silt at the upper part of the profile.  $M_1$ , grey and black, mean grain-size is  $5.14\Phi$ , sand was more at the top and the bottom parts of the profile, whereas silt is more in the middle parts. YM, brown in color, mean grain-size is  $4.96\Phi$  and mean grain-size aggrandizes from top to bottom, sediment is mainly composed of silt and sand, and sand composition is reducing from bottom to top parts of the profile. Y, snuff color, mean grain-size is  $5.01\Phi$  and grain-size becomes much thinner from the bottom to the top, mail component is silt, and residual vegetation roots are found in the profile. YL, brown-yellow, silt-mud mixed, mean grain-size is  $4.63\Phi$ , mainly composed of silt and sand. L, brown-yellow, the *Phragmites australis* roots are found in the whole profile, mean grain-size is  $4.63\Phi$ , mainly composed of silt.

#### 4.1.2 Comparison of frequency curves and standard deviations

It is obvious with the evidence that the distribution of the grain-size changing in depth, which may reflect the grain-size characteristics in different phases of the tidal flat evolution. The same characteristics of grain-size are found in different depths of those cores. To better understand the grain-size characteristics, sediment cores (G, M, YM, Y) that have similar grain-size parameters are selected to make the analysis. Typical grain-size frequency curves are compared with each other, and the results indicate that these cores have similar typical grain-size frequency curves. The typical grain-size frequency curves of G, M and YM have one or two phases that correspond to the frequency curve of M (Figure 3—grain-size frequency curves). Former reports on the vegetation evolution on the tidal flat (Yang *et al.*, 2002) claimed that the introduction of the *Spartina angilica* was in the 1990s, after then the *Spartina angilica* covered almost all of the middle parts of the tidal flat. The *Spartina alterniflora* was introduced to the area in the 1980s, after then the *Spartina alterniflora* clustered within a width of 500 m in the lower part of the tidal flat. At present, *Spartina angilica* is disappearing because of the invasion of the *Spartina alterniflora*. The *Spartina alterniflora* is also the pioneer plant on the tidal flat nowadays. Integrating the grain-size distribution information and the evolution phases of the tidal flat, one conclusion is made that the silt tidal flat experiences from silt tidal flat to the *Spartina angilica* tidal flat, and then to the silt tidal flat. The *Spartina alterniflora* tidal flat, the *Suaeda salsa* tidal flat and the transitional zone of *Spartina alterniflora* and *Suaeda salsa* experience from the *Spartina angilica* tidal flat to the *Spartina alterniflora* tidal flat, the *Suaeda salsa* tidal flat to the *Spartina angilica* tidal flat to the *Suaeda salsa* tidal flat, the *Suaeda salsa* tidal flat to the *Spartina angilica* tidal flat to the transitional zone of *Suaeda salsa* and *Spartina alterniflora*, respectively.

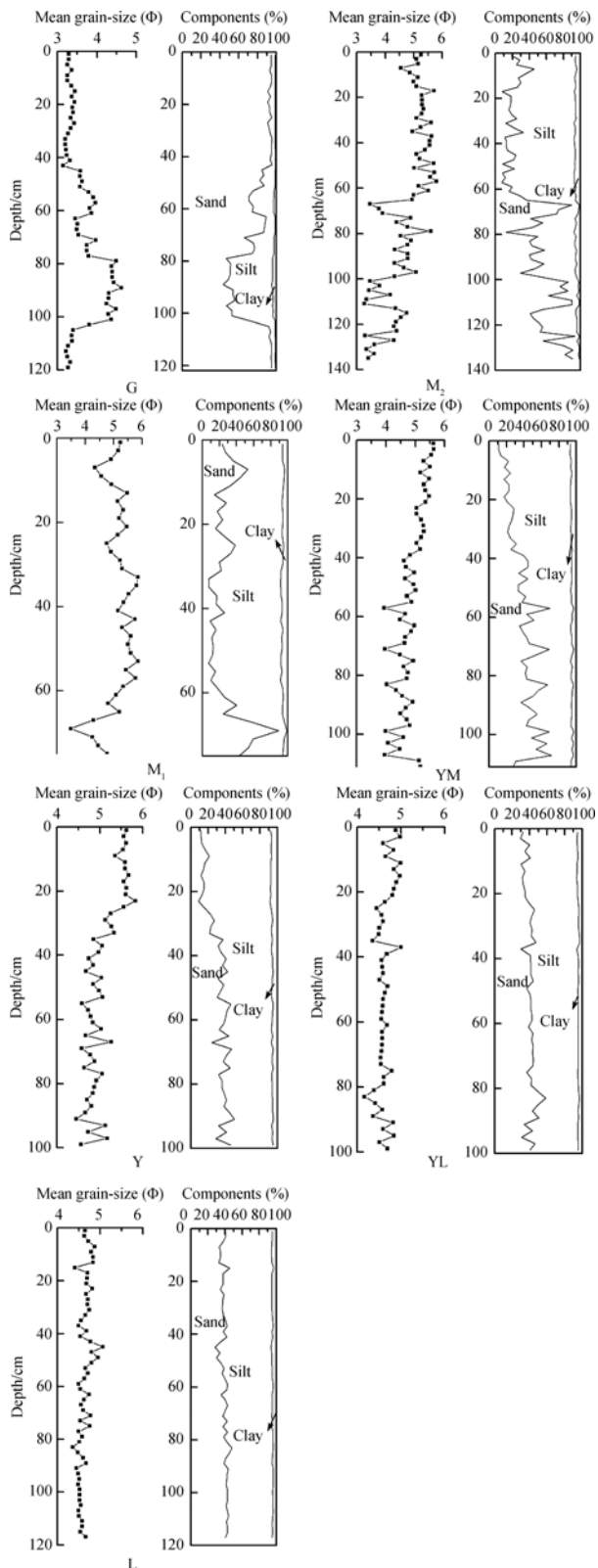
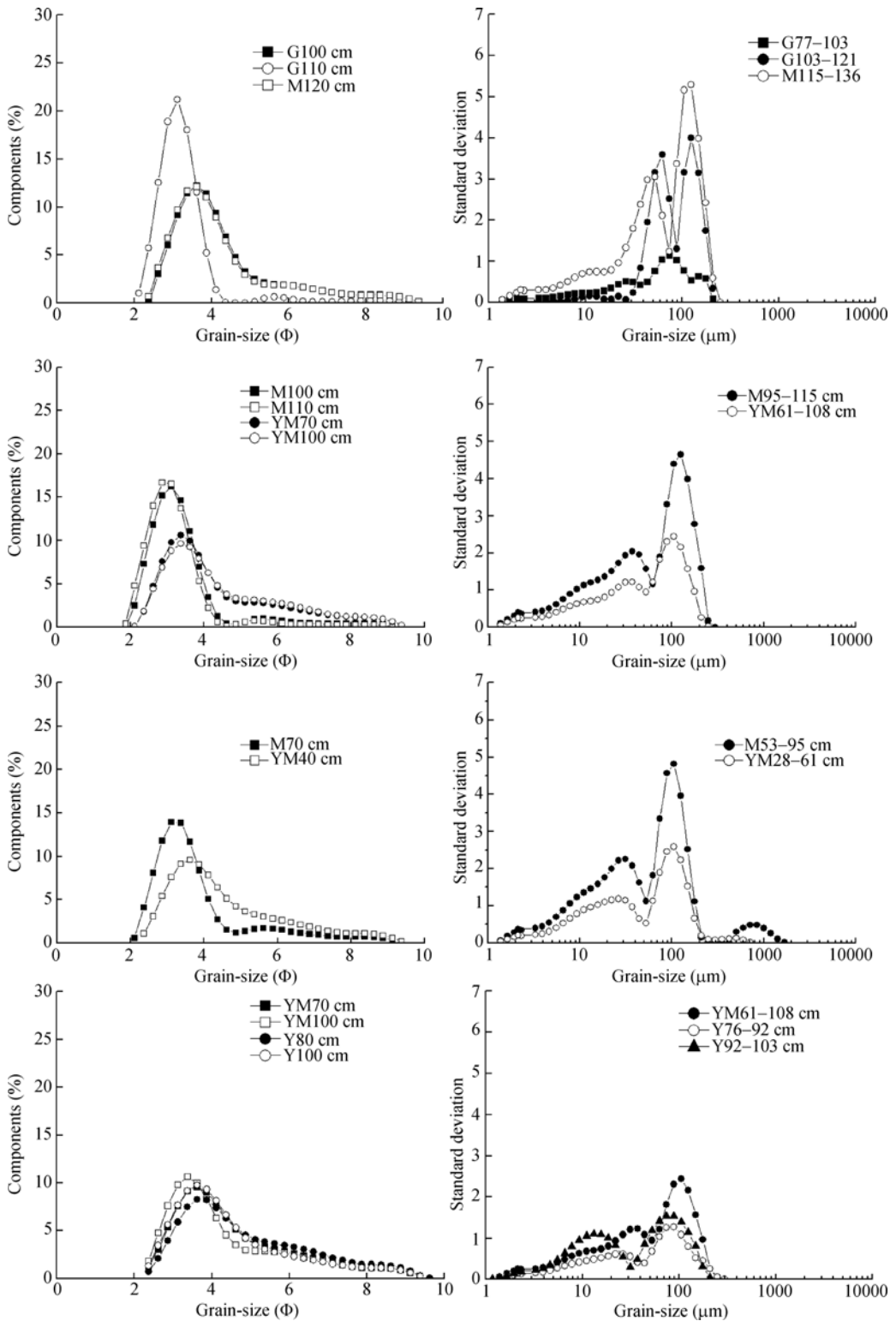


Figure 2 The vertical distribution of mean grain-size and components for sediment cores



**Figure 3** Comparison of different depths among cores (left: grain-size frequency curves; right: standard deviations of grain-size components)

If sediment source is constant and stable, the most important reason to influence the grain-size distribution is the hydrodynamics. The high content of suspended sediment occurs in the lower part of the tidal flat at Xinyanggang, and the content is reducing dramatically toward the higher part of the tidal flat (Zhang, 1986; Li *et al.*, 2007). The hydrodynamics is gradually losing its power from sea to land. The grain-size standard deviations in different depths of G, M, YM and M are compared (Figure 3—standard deviations of grain-size components), the grain-size components which have high value of grain-size standard deviations are those that have high environment sensitivity (Wang *et al.*, 1999; Sun *et al.*, 2003). The grain-size standard deviations of G, M, YM and Y all have peak values corresponding to coarse or fine sediment, and the cores experiencing the same evolution phases have similarly standard deviation curves. The grain-size distribution information in fact reflects that different tidal zones response to different hydrodynamics on the tidal flat and the hydrodynamics is intense in the lower part of the tidal flat. The frequency of tidal inundation in different tidal zones (G, M, YM, Y, YL and L) is >80%, 50%–80%, 40%–60%, 20%–50%, 5%–20%, <5%, respectively (Yang, 2002).

Tidal flat is widely distributed at Xinyanggang, belonging to accretion coastal area, waterline of mean high water level is still advancing to the sea (Zhang *et al.*, 2002). Vegetation influenced the transportation of the suspended sediment and the velocity of flow on the tidal flat (Gao *et al.*, 2005; Wang *et al.*, 2006). Top sediment grain-size analysis at seven stations of the sediment cores reflected that sediment was coarse at silt-fine sand tidal flat, median at *Spartina alterniflora* tidal flat and fine at *Suaeda salsa* tidal flat (Table 1). Hydrodynamics varied from sea to land may be the controlled element, and vegetation growth impelled the same grain-size to accumulate into different zones of the tidal flat.

#### 4.2 Characteristics of spatial distribution of $^{137}\text{Cs}$ and $^{210}\text{Pb}$ at the surface of the sediment

The activities of  $^{137}\text{Cs}$  and  $^{210}\text{Pb}$  at the surface of the sediment are shown in Figure 4. The activities of  $^{137}\text{Cs}$  and  $^{210}\text{Pb}$  change spatially according to the sediment zones. The activity of  $^{137}\text{Cs}$  in silt-fine sand and mud-sand mixed zone is undetectable and increasing from sea to land gradually, reaching 3.12 Bq/kg in the *Phragmites australis* zone. Whereas, the activity of  $^{210}\text{Pb}$  at silt-fine sand and mud-sand mixed zone is 18.75 Bq/kg and decreases toward the *Spartina alterniflora* zone, after which a minimum over the broad zone of *Spartina alterniflora* and the transitional zone of *Suaeda salsa* and *Spartina alterniflora* is observed. Activity of  $^{210}\text{Pb}$  increases to a peak of 26.12 Bq/kg in the *Phragmites australis* and *Suaeda salsa* transitional zone, and decreases to 20.12 Bq/kg in the *Phragmites australis* zone. Most of  $^{137}\text{Cs}$  is attached to fine-grained sediments, especially in clay, and stable in

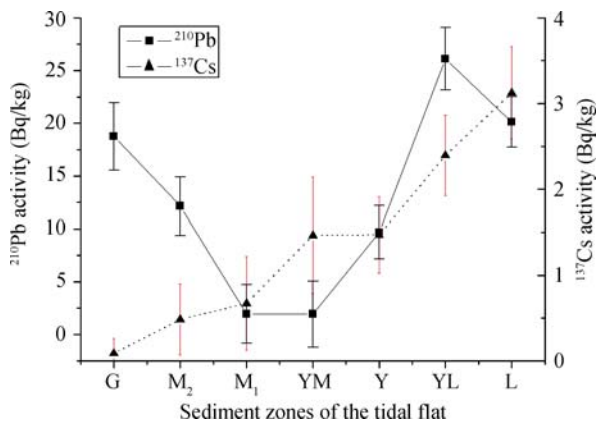


**Figure 4**  $^{210}\text{Pb}$  and  $^{137}\text{Cs}$  spatial distribution in the top sediment at Xinyanggang

the sediment although the possibility of diffusion in the sediment (Wan, 1995; Goff, 1997). The activities of  $^{137}\text{Cs}$  and  $^{210}\text{Pb}$  variation at the surface of the sediment have no correlation ( $R=0.52$  &  $0.53$ ,  $n=7$ ) with the variation of sediment grain-size according to the spatial distribution of sediment zones of the tidal flat (Table 1).

**Table 1** Grain-size parameters and components for surface sediments

Samples	Mean size ( $\Phi$ )	Sorting coefficient	Skewness	Kurtosis	Sand (%)	Silt (%)	Clay (%)
G	3.29	0.89	1.38	1.89	94.77	4.12	1.11
M <sub>2</sub>	5.26	1.40	1.26	1.83	18.19	76.36	5.45
M <sub>1</sub>	5.13	1.48	1.28	1.95	27.39	66.38	6.21
YM	5.62	1.36	1.03	1.76	10.70	82.74	6.56
Y	5.63	1.42	1.10	1.81	11.53	80.83	7.64
YL	4.88	1.50	1.41	2.01	32.40	62.49	5.11
L	4.64	1.47	1.52	2.05	40.25	55.21	4.54

The factors influence the accumulation of  $^{210}\text{Pb}$  include sediment grain-size and content of organic matters (Wang *et al.*, 2005). The source of organic matters in the silt-fine sand and mud-sand mixed zone and the *Phragmites australis* zone mainly come from the sea, but the zone of *Spartina alterniflora* and the transitional zone of *Suaeda salsa* and *Spartina alterniflora* mainly come from land (Gao *et al.*, 2005), and the organic content on the tidal flat is fluctuated in different zones (Gao *et al.*, 2007), which may explain the non-steady state of  $^{210}\text{Pb}$  activity at the surface of the sediment.

### 4.3 The profile of $^{137}\text{Cs}$ and its sedimentary environment implication

#### 4.3.1 The profile of $^{137}\text{Cs}$ and sediment rate

The vertical profiles of  $^{137}\text{Cs}$  activity of the sediment cores are shown in Figure 5. G is located in the lower part of the intertidal zone, undergoing the strongest hydrodynamics in the tidal flat, intensive deposition and erosion process occurred periodically and the process conversion happened within a short time. It's hard to detect the activity of  $^{137}\text{Cs}$  at silt-fine sand and mud-sand mixed tidal flat.

The activity of  $^{137}\text{Cs}$  drastically changes from surface to 35 cm in the core of M<sub>2</sub>. However, in the lower part of the profile, three sequential peaks are observed. The maximum peak is also the depth with the maximum activity of  $^{137}\text{Cs}$  (1.53 Bq/kg), the  $^{137}\text{Cs}$  activity at the bottom of the profile is 0.39 Bq/kg, not reaching its origination detectable depth. Supposing the values of three peaks can be used for chronology, taking the maximum peak as originating from 1964, two other sub-peaks corresponding to 1974 and 1986, respectively (Figure 5-M<sub>2</sub>), sediment rate can speculate on the hypothesis. Sediment rate in this area from 1986 to 2007 is 4 cm/a, that from 1974 to 1986 is 2.0 cm/a, and from 1964 to 1974 is 2.2 cm/a. The sediment rate is approximately as the same as the rate at the *Spartina alterniflora* flat of 3.0 cm/a on Xinyanggang tidal flat (Yang *et al.*, 2002). Dating of sediment core that is also located at the *Spartina alterniflora* flat has been undertaken in Wanggang (Wang *et al.*, 2005), which is only 50 km in distance. These two have similar vertical profiles of  $^{137}\text{Cs}$  activity in the same depth, and the sediment rates calculated from dating of  $^{137}\text{Cs}$  have the similar results. Based on the sediment rate, texture and grain-size distribution of the

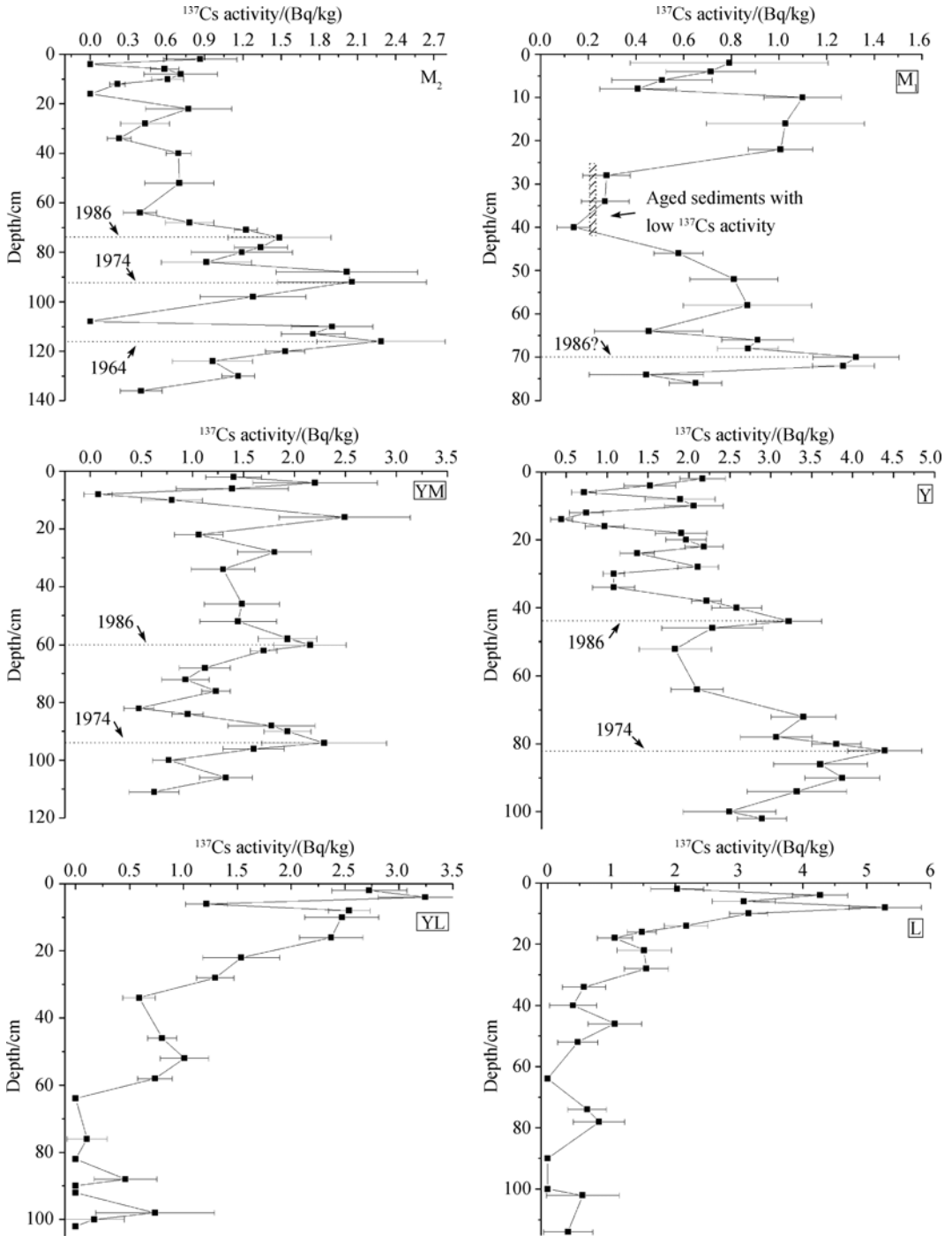


Figure 5 <sup>137</sup>Cs profiles of the cores at Xinyanggang

sediment, roots residual abundant at the depth of 30–60 cm and grain-size transform to thinner up the depth of 60 cm, 60 cm may be the evolution interface (from silt-fine sand and mud-sand mixed zone to the *Spartina alterniflora* zone) of the tidal flat.

M<sub>1</sub> is 200 m from M<sub>2</sub> in distance, and the vertical profile of <sup>137</sup>Cs shows very low activity

of  $^{137}\text{Cs}$  over the depth interval of 30–40 cm. Limited by the depth of the profile, only one peak of  $^{137}\text{Cs}$  is found in the core. Referencing to  $M_2$ , taking the maximum  $^{137}\text{Cs}$  activity in the profile as originating from 1986 (Figure 5– $M_1$ ), sediment rate from 1986 to 2007 is 3.5 cm/a.

Core YM is located in the *Suaeda salsa* and *Spartina alterniflora* transitional zone, *Spartina alterniflora* is clustered on the mass *Suaeda salsa* flat. Vertical profile of  $^{137}\text{Cs}$  shows a high activity of  $^{137}\text{Cs}$  at the depth of 20 cm, this may be caused by sediment mixing and should be omitted when dating. It shows a peak at a depth of 60 cm and another peak at 94 cm depth. Deeper  $^{137}\text{Cs}$  peak may be present but limited by the depths of the core. Given that the first peak is corresponding to 1986, and another peak is corresponding to 1974 (Figure 5–YM), then the sediment rate from 1974 to 2007 is 2.8 cm/a, from 1986 to 2007 is 2.7 cm/a, and from 1974 to 1986 is 3.0 cm/a.

Y is located in the middle part of the *Suaeda salsa* flat. Vertical profile of  $^{137}\text{Cs}$  in the upper layer of the profile is as similar as that in the former sediment core.  $^{137}\text{Cs}$  activity shows peaks at 40 cm and at 90 cm in depth. With respect to YM, a hypothesis could be made. The first peak can be explained by the atmospheric fallout from the Chernobyl accident in 1986 and the other peak will be corresponded to the atmospheric fallout from the nuclear weapon test in the 1970s (Figure 5–Y). Additionally, a more distinct peak will exist below the two peaks but not be found due to the limited depths. Based on the peaks, sediment rate from 1986 to 2007 is 1.9 cm/a, and from 1974 to 2007 is 2.7 cm/a, from 1974 to 1986 is 4.1 cm/a. Similarly, considering the roots residual of *Suaeda salsa* in YM at 28 cm and *Spartina* at 60 cm in depth, combined with the sediment rates, sediment texture and grain-size distribution, the time of the *Spartina* tidal flat evolution to the *Suaeda salsa* tidal flat is 1997 in this zone. For Y, roots residual of *Suaeda salsa* at 76 cm and *Spartina* at 82 cm in depth, the time of *Spartina* flourishing in this zone is in 1978. After the extending of *Spartina*, which accelerated the accretion, so the high sediment rate of 3–4.1 cm/a of YM and Y from 1974 to 1986 is reasonable.

YL, *Phragmites australis* is clustered on the mass *Suaeda salsa* tidal flat. Vertical profile of  $^{137}\text{Cs}$  is distinguished from the former sediment cores. Activity of  $^{137}\text{Cs}$  is reducing from surface down to the depth of 30 cm gradually and smoothly, no subsurface  $^{137}\text{Cs}$  maximum is observed. At the depth of 90 cm it shows the penetration depths (Figure 5–YL). The  $^{137}\text{Cs}$  activity of 1 Bq/kg below the depth may be explained by post-deposition mixing. Taking the penetration depths as corresponding to 1954, the sediment rate is 1.2–1.7 cm/a from 1954 to 2007.

L, is located on the flourish *Phragmites australis* tidal flat. Vertical profile of  $^{137}\text{Cs}$  is as similar as that at YL, and taking the depths of 64 or 90 cm as penetration depths, the sediment rate at this area is 1.2–1.7 cm/a from 1954 to 2007.

Liu *et al.* (2008) reported that sediment rate based on grain-size distribution on Xinyanggang tidal flat is between 2.1 and 3.1 cm/a. Wang *et al.* (2005) reported that sediment rate based on  $^{137}\text{Cs}$  and  $^{210}\text{Pb}$  dating on Wanggang tidal flat, the tidal flat experienced different sediment rates between 2.0 and 4.2 cm/a in different phases. Yang *et al.* (2002) reported that sediment rate based on topography measurement (from 1980 to 1992) on Xinyanggang tidal flat is between 1.5 and 3.0 cm/a. Our data showed a good agreement with the previous study (Table 2). The chronology of each core indicated spatial and temporal variability of natural

influences on sedimentation.

#### 4.3.2 Environment implication of the $^{137}\text{Cs}$ profiles

Vertical profiles of  $^{137}\text{Cs}$  of  $M_2$ ,  $M_1$ , YM and Y are fluctuated from the surface to 30 or 40 cm sect in depths. Based on the sediment rate, the 30 or 40 cm depths of the core are corresponding to the sedimentary time of 1999, 1997, 1996 and 1992. The time probably matched to the phases that the *Spartina alterniflora* were extending on the different zones of tidal flat. Because *Spartina alterniflora* has a tremendous ability to absorb grain-fine sediments and organic matters (Gao *et al.*, 2005; Gao *et al.*, 2007), and  $^{137}\text{Cs}$  is preferentially held onto clay and organic particles and is strongly adsorbed to cation-exchange sites (Goff, 1997), so  $^{137}\text{Cs}$  is accumulated at these depths of the cores.

Table 2 shows the  $^{137}\text{Cs}$  characteristics of the sediment cores. The  $^{137}\text{Cs}$  maximum in the profiles will correspond to the year of 1963, 1974 or 1986, which reflects by the peaks of  $^{137}\text{Cs}$  activity in the sediment cores if it's in a stabilized sedimentary environment and  $^{137}\text{Cs}$  will occur in the correct age horizons. The cores of  $M_2$ ,  $M_1$  and Y are matched well. The  $^{137}\text{Cs}$  maximum in the profile of YM at the depth of 16 cm may be caused by extensive accretion or erosion process, which brings external material into the core. The  $^{137}\text{Cs}$  maximum in the cores are increasing gradually from  $M_2$  to (except for  $M_1$ ) L, agreement with the theory that high  $^{137}\text{Cs}$  radioactivity related to low sediment rate (Milliman, 1985). Ratios of peaks for 1986/1974 are 0.83, 0.83 and 0.61, respectively. The coherence and comparable results were similar to the reports in areas (estuaries, coastal areas) where round vertical profiles of  $^{137}\text{Cs}$  were preserved in the sediment (Pan *et al.*, 2008). Based on the analysis, sediment rates calculated on the  $^{137}\text{Cs}$  peaks are accurate.

**Table 2** Distribution characteristic of  $^{137}\text{Cs}$  distribution in sediments of tidal flat of Xinyanggang

Stations	$^{137}\text{Cs}$ activity (Bq/kg)		Depth of $^{137}\text{Cs}$ maximum (cm)	Depth of peak of $^{137}\text{Cs}$ activity (cm)	Detectable depth of $^{137}\text{Cs}$ activity (cm)	Ratios of peaks for 1986/1974	Sediment rate after 1986 (cm/a)
	Max	Min					
$M_2$	1.53	0	120	120	>136	0.83	4
$M_1$	1.12	0.13	70	70	>70	–	3.5
YM	2.49	0.07	16	94	>111	0.83	2.7
Y	3.87	0.44	90	90	>100	0.61	1.9
YL	3.24	0	4	–	60-90	–	1.2–1.7
L	5.28	0	8	–	60–90	–	1.2–1.7

#### 4.4 The profile of $^{210}\text{Pb}$ and its sedimentary environment implication

The vertical profiles of  $^{210}\text{Pb}$  in the sediment cores have different types (Wang, 1997; Fan *et al.*, 2000). An ideal expect exponential decrease in  $^{210}\text{Pb}$  activity with depth can be used to estimate sediment accretion rates, assuming there is uniform and constant input of lead to sediment surface, and a constant accretion rate (Joanna, 2008). A mixed sect would be found in the profile if the sediment is experienced pre-deposition and post-deposition through hydrodynamics or bioturbation. Sediment contained only the  $^{210}\text{Pb}$  activity derives from the decay of its parent  $^{226}\text{Ra}$ , then, the profile can be seen as a background sect. So a vertical profile of  $^{210}\text{Pb}$  may contain decreased, mixed and background sect. With  $^{210}\text{Pb}$  activity

similarly within the whole vertical depths, sediment must be suffered strong mixed force, no net vertical accretion or extremely rapid sediment accumulation rate occurred. Linear or erratic profiles of  $^{210}\text{Pb}$  may be explained by an accident event in geology, complex hydrodynamics and uneven sedimentary environment or rapid changes in sediment supply/or energy conditions (Andrew *et al.*, 2003).

Vertical profiles of  $^{210}\text{Pb}$  are shown in Figure 6. Fluctuated profiles of  $M_2$ ,  $M_1$ , YM and Y reflect the sedimentary environment varying vigorously in short time, sediment mixed extensively. The very low  $^{210}\text{Pb}$  activity at the depth of 20–40 cm in  $M_1$  (the situation also can be seen in their  $^{137}\text{Cs}$  profiles, Figure 5) must be aged sediment as mentioned by Thorbjorn *et al.* (2000). However, YL and L have distinguishable profiles,  $^{210}\text{Pb}$  activity presented at the sediment surface, with a sharp decline to zero activity within the top few depths (the situation also can be seen in their  $^{137}\text{Cs}$  profiles, Figure 5). Prolonged erosion or repeated dredging that completely remove recent sediments, exposing older deposit (Andrew *et al.*, 2003) and reclamation in the high part of the tidal flat may lead to the result. Evidence is obvious because of being near the core station, landscape was reshaped by anthropogenic activities. Distance from the core of YL is about 20 m, a dyke with a height approximately 50 cm is constructed to control the tidal water. The core at L is surrounded by dykes, with 40 cm depth of water in the area. Aquafarm was built from the last century near the levee of the coast. The two cores (YL and L) near the levee become an isolated ecosystem and out of the effects of tidal hydrological control, minimum sediment rates of 0.03 cm/a at the top of the cores calculated by CIC method reflected the real low deposition rate of sedimentary environment. As a whole, CIC method is difficult to apply to the  $^{210}\text{Pb}$ -profiles on the intertidal sediments mainly because of the higher rate of reworking of the sediment and the extensively tidal range and hydrodynamic force. So sediment rate of 1.2–1.7 cm/a speculated on  $^{137}\text{Cs}$  profile is underestimated the real accretion rate in the area.

The sediment cores at  $M_2$ ,  $M_1$ , YM and Y display  $^{210}\text{Pb}$  fluctuations with depths on the tidal flat, which apparently render the  $^{210}\text{Pb}$ -CIC method invalid. The  $^{210}\text{Pb}$ -CRS model assumes a constant rate of supply of unsupported  $^{210}\text{Pb}$  to the sediment surface despite variable sedimentation rates and any deviation from an exponential decrease of the unsupported  $^{210}\text{Pb}$  with depth represents a real change in accumulation rate (Adam *et al.*, 2008). The CRS method is able to evaluate the ages at various depths in the core, and hence the sedimentation rates between the depth intervals (Shigeru *et al.*, 2006). Sediment source material is alternative, and the sediment rate varies in different evolution phases of the tidal flat. For those reasons, CRS method is applied to the four cores on the tidal flat and the sediment ages are compared with the ages calculated from  $^{137}\text{Cs}$  dating, and the  $^{137}\text{Cs}$  peaks corresponded to the symbol years of maximum fallout from atmospheric weapons testing are marked as circles in depths of the cores (Figure 7). The ages are consistent in the upper depths of the cores but increasing distinction to the lower depths of the cores. Sameness ages are observed at the surface to the depths of 70 cm, 40 cm, 90 cm and 40 cm of the  $M_2$ ,  $M_1$ , YM and Y, respectively. However, under these depths the ages calculated from CRS method are much order than the age from  $^{137}\text{Cs}$  dating. On the tidal flat environment, the sediment flux is constant, but the flux of unsupported  $^{210}\text{Pb}$  and the supported  $^{210}\text{Pb}$  activity (both of which may slightly affect ages given by CRS method) may be various caused by difference

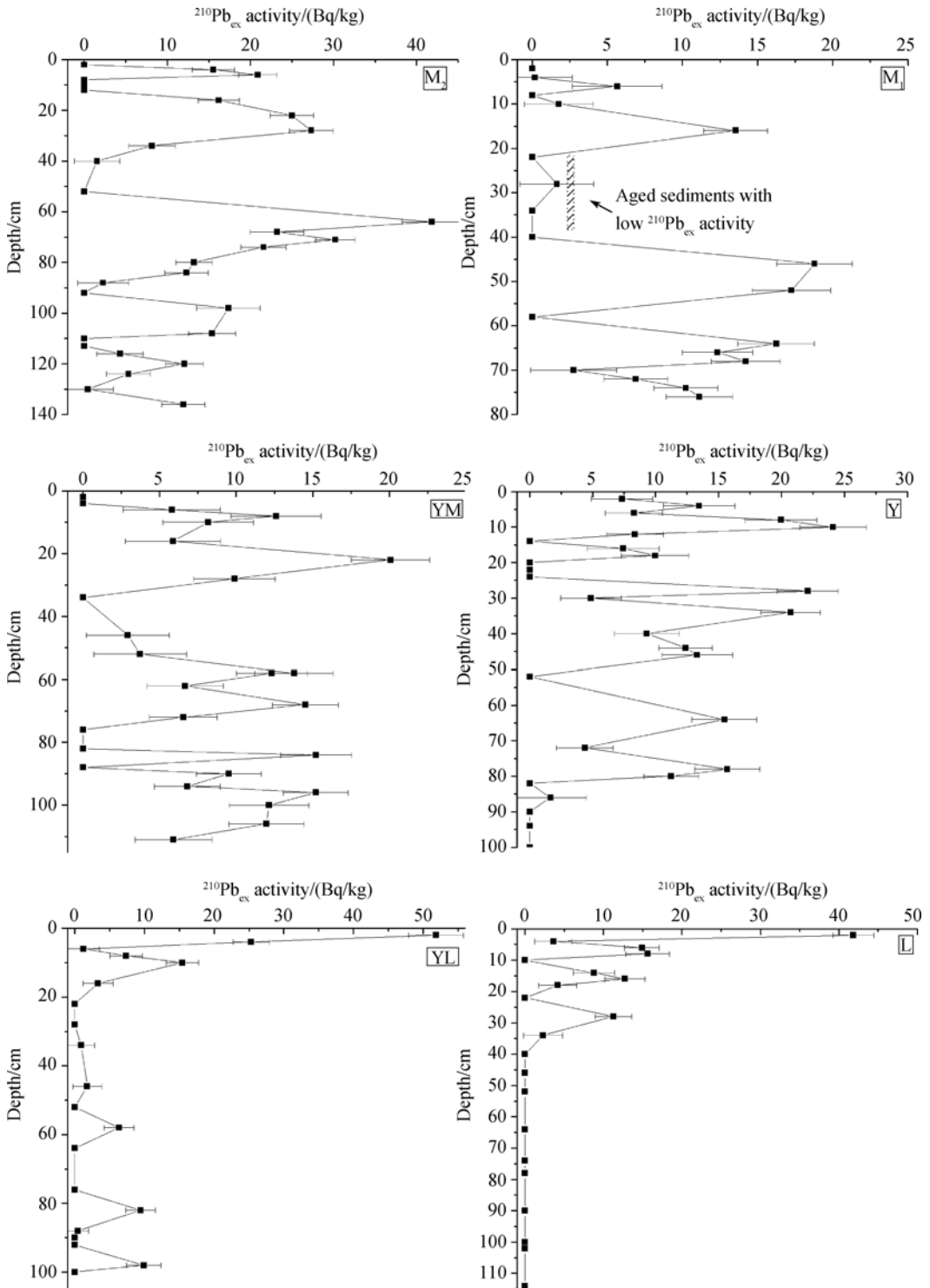


Figure 6  $^{210}\text{Pb}_{\text{ex}}$  profiles of the cores at Xinyanggang

of sediment source and composition, the distribution of unsupported  $^{210}\text{Pb}$  in the profile is not steady as a result of that (Lin *et al.*, 1998; Andrew *et al.*, 2003). Additionally, in the

lower depths of the cores where  $^{210}\text{Pb}$  activity decreases with depth, the changes become very important beyond the analytical errors and the  $^{210}\text{Pb}$ -derived age cannot be used (Kang, 1986). The average sedimentation rates based on the  $^{210}\text{Pb}$  for the four cores are calculated to be 3.5, 3.1, 2.5 and 1.9 cm/a, respectively, which are comparable with the rates of 4, 3.5, 2.7 and 1.9 cm/a based on the  $^{137}\text{Cs}$  method. The two methods can be cross-checked with each other, the sediment rate made from the radiochronology was reasonable on the tidal flat.

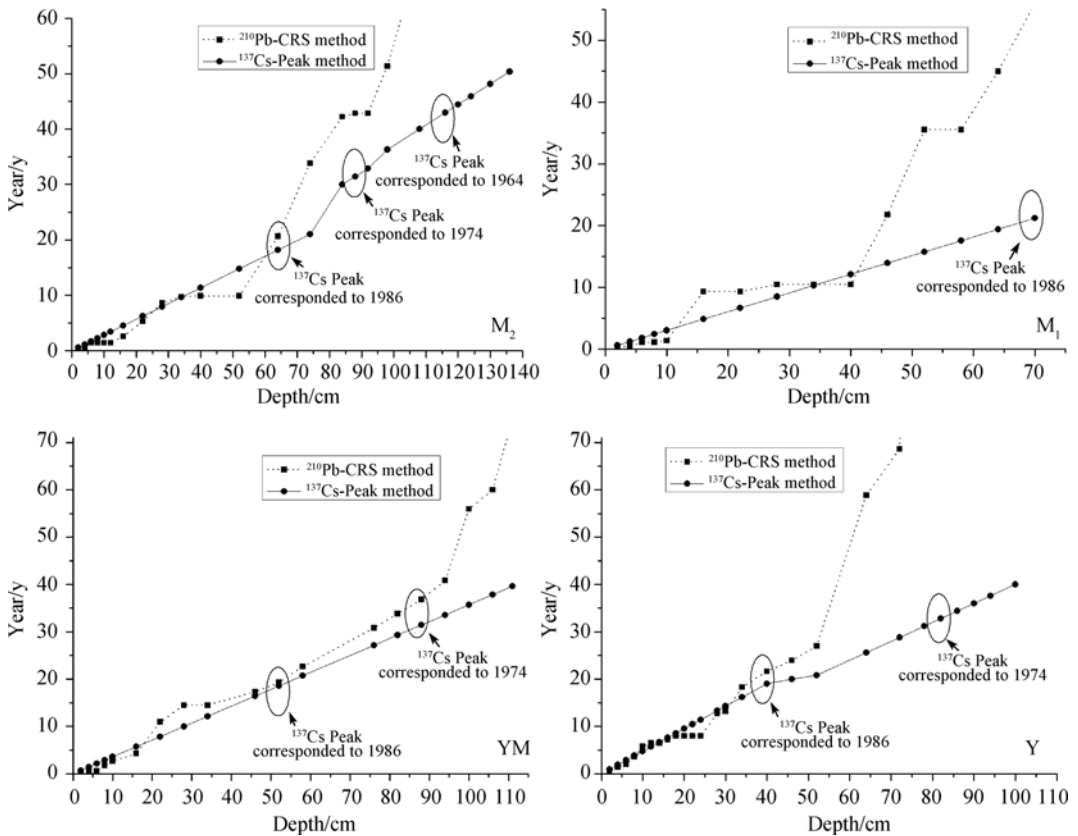


Figure 7 Age vs. depth of the cores at Xinyanggang

#### 4.5 Stratigraphy and evolution line of the tidal flat

Considering the grain-size distribution information, texture of the profiles, sediment rates of the cores and topography of the tidal flat, stratigraphy and evolution lines of the tidal flat are built (Figure 8). *Spartina alterniflora* zone has the highest elevation on the tidal flat. The elevation slowly decreases from land to *Suaeda salsa* zone, quickly increases about 8 cm to the *Spartina alterniflora* zone and sharply decreases to the sea (Bai, 2008). The tidal flat is convex in shape, reflecting the accretion environment. High elevation at *Phragmites australis* zone reflects that the *Phragmites australis* vegetation obtains strong sediment absorption ability on the tidal flat. Four evolution lines represent the surface layer of the cores in different years. Evolution lines of 1986 and 1997 with a steeper slope between Y and G than that of 1964 and 1974 reflect a higher accretion rate after introducing of *Phragmites* to the tidal flat in those years.

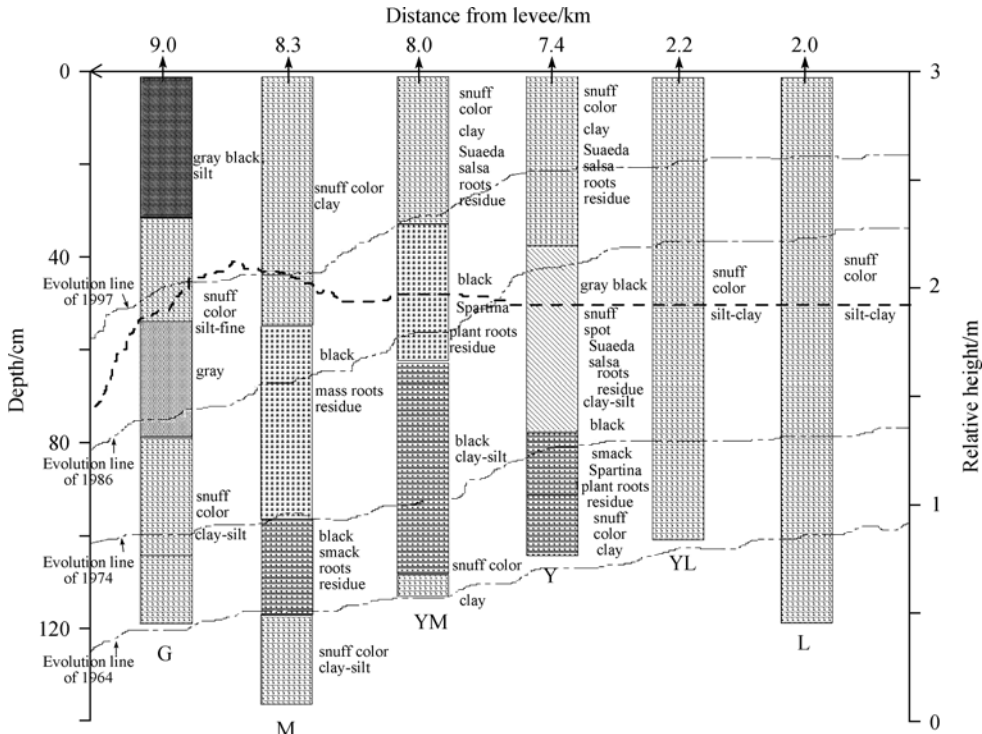


Figure 8 Stratigraphy and evolution line (relative to depth of every core) of the tidal flat at Xinyanggang

## 5 Conclusions

(1) Grain-size distribution analysis of the sediment cores showed that different tidal zones experienced various evolution phases. Typically the *Spartina alterniflora* tidal flat experienced from the *Spartina anglica* tidal flat to the *Spartina alterniflora* tidal flat. In the process of tidal flat evolution, each tidal zone responds to the hydrodynamic variation while the lower part of the tidal flat has the mostly fierce response to it. So the coarse-fine variety of sediments changed horizontally from the silt-fine sand tidal flat to the *Spartina alterniflora* tidal flat and the *Suaeda salsa* tidal flat gradually. Vegetation cover on the tidal flat impelled the process, which was evidently reflected on the grain-size distribution of surface sediments.

(2) The activities of  $^{137}\text{Cs}$  and  $^{210}\text{Pb}$  at the surface of the sediment were examined. The result showed that activities of  $^{137}\text{Cs}$  and  $^{210}\text{Pb}$  at the surface of the sediment have no correlation with the sediment grain-size distribution. The factor influenced the accumulation of  $^{210}\text{Pb}$  on the tidal flat may be more complex.

(3) The vertical profiles of  $^{137}\text{Cs}$  were accountable for chronology on the tidal flat. After covering the *Spartina alterniflora*, the pioneer vegetation extensively absorbed fine-grained sediments on the tidal flat and caused the fluctuated of  $^{137}\text{Cs}$  activity in the upper profiles. The characteristics of  $^{210}\text{Pb}$  profiles reflected the variously sedimentary environment of the tidal flat. Vertical profiles of  $^{210}\text{Pb}$  reflected the repeated cycles of hydrodynamics on tidal flat, the  $^{210}\text{Pb}$  activity decreased abruptly within top depths of the sediment and the same situation to the end showed a nearly isolated hydrodynamics and anthropogenic influence on the environment. CRS method was suited to chronology on the tidal flat. The ages calculated

from  $^{210}\text{Pb}$  and  $^{137}\text{Cs}$  dating were comparable and were consistent with the former reports. Both of the  $^{210}\text{Pb}$  and  $^{137}\text{Cs}$  profiles give exuberance information on the hydrodynamic, bioturbation and phyturbation variations of the deposition process. Integrating the information of grain-size distribution, texture of the profiles, sediment rates of the cores and topography of the tidal flat, evolution lines of the tidal flat were reconstructed.

(4) In conclusion, the combination of radionuclide dating of sediment with information on the grain-size distribution analysis was a reliable method of determining the sedimentary environment and evolution phases of the tidal flat.

## References

- Adam A A, Bassam G, Michelle G *et al.*, 2008. Recent peat accumulation rates in minerotrophic peatlands of the Bay James region, Eastern Canada, inferred by  $^{210}\text{Pb}$  and  $^{137}\text{Cs}$  radiometric techniques. *Applied Radiation and Isotopes*, 66: 1350–1358.
- Andrew B C, Lan W C, Alejandro C *et al.*, 2003. Reconstructing historical trends in metal input in heavily-disturbed, contaminated estuaries: Studies from Bilbao, Southampton Water and Sicily. *Applied Geochemistry*, 18: 311–325.
- Bai Fenglong, 2008. Carbon–nitrogen accumulation patterns of the Xinyanggang tidal flat deposits, central Jiangsu coast, eastern China. Nanjing: Nanjing University Thesis, 22–28. (in Chinese)
- Chanton J P, Martens C S, Kipphut G W *et al.*, 1983. Lead-210 sediment geochronology in a changing coastal environment. *Geochemical Cosmochimica Acta*, 47: 1791–1804.
- Chen Caijun, 1991. Development of depositional tidal flat in Jiangsu Province. *Oceanologia et Limnologia Sinica*, 22(4): 360–368. (in Chinese)
- David A D, Steven A K, 1995. Non-steady-state  $^{210}\text{Pb}$  flux and the use of  $^{228}\text{Ra}/^{226}\text{Ra}$  as a geochronometer on the Amazon continental shelf. *Marine Geology*, 125: 329–350.
- Fan Dejiang, Yang Zhuosheng, Guo Zhigang, 2000. Review of  $^{210}\text{Pb}$  dating in the continental shelf of China. *Advance in Earth Sciences*, 15(3): 297–302. (in Chinese)
- Gao Jianhua, Bai Fenglong, Yang Guishan *et al.*, 2007. Distribution characteristics of organic carbon, nitrogen, and phosphor in sediments from different ecological zones of tidal flats in north Jiangsu Province. *Quaternary Sciences*, 27(5): 756–765. (in Chinese)
- Gao Jianhua, Yang Guishan, Ou Weixin, 2005. Analysizing and quantitatively evaluating the organic matter source at different ecologic zones of tidal salt marsh, north Jiangsu Province. *Environmental Science*, 26(6): 51–56. (in Chinese)
- Gao Shu, 2009. Modeling the preservation potential of tidal flat sedimentary records, Jiangsu coast, eastern China. *Continental Shelf Research*, doi:10.1016/j.csr.2008.12.010
- Goff J R, 1997. A chronology of natural and anthropogenic influences on coastal sedimentation, New Zealand. *Marine Geology*, 138: 105–117.
- Guebuem K, Najid H, Thomas M C *et al.*, 1997. The fallout isotope  $^{207}\text{Bi}$  in a Delaware salt marsh: A comparison with  $^{210}\text{Pb}$  and  $^{137}\text{Cs}$  as a geochronological toll. *The Science of the total Environment*, 196: 31–41.
- Joanna C E, 2008. Long-term retrospection on mangrove development using sediment cores and pollen analysis: A review. *Aquatic Botany*, 89: 93–104.
- Kang Xinglun, 1986. On the data treatment of  $^{210}\text{Pb}$  dating method. *Marine Sciences*, 10(6): 13–17. (in Chinese)
- Ke Xiankun, 1993. The ecological system and the exploitation model of tidal flats: A case study of the tidal flats of Defeng County, Jiangsu Province. *Journal of Natural Resources*, 8(2): 122–131. (in Chinese)
- Li Zhanhai, Gao Shu, Chen Shenliang, 2007. Characteristic of grain size distributions of seabed and suspended sediment over the Dafeng tidal flat of Jiangsu Coast. *Journal of Sediment Research*, 3: 30–37. (in Chinese)
- Lin Ruifen, Min Yushun, Wei Keqin *et al.*, 1998.  $^{210}\text{Pb}$ -dating of sediment cores from the Pearl River mouth and its environmental geochemistry implication. *Geochimica*, 27(5): 401–411. (in Chinese)
- Liu Xuying, Gao Jianhua, Bai Fenglong *et al.*, 2008. Grain size information in different evolution periods of Xinyanggang tidal flat in Jiangsu Province. *Marine Geology and Quaternary Geology*, 28(4): 27–35. (in Chi-

- nese)
- Mcmanus J, 1988. Grain Size Determination and Interpretation, Techniques in Sedimentology. Oxford: Blackwell, 63–85.
- Milliman J D, Shen H T, Yang Z S *et al.*, 1985. Transport and deposition of river sediment in the Changjiang estuary and adjacent continental shelf. *Continental Shelf Research*, 4(1/2): 37–45.
- Nriagu J O, 1978. The Biogeochemistry of Lead in the Environment. New York: North-Holland Biomedical Press, 287–300.
- Pan Shaoming, Guo Dayong, Liu Zhiyong, 2008. Sedimentation and erosion in Pui O salt marsh of Hong Kong from  $^{137}\text{Cs}$  distribution in sediment. *Acta Sedimentologica Sinica*, 26(4): 655–660. (in Chinese)
- Pan Shaoming, Zhu Dakui, Li Yan *et al.*, 1997. Cs-137 profile in sediments in eustuaries and its application in sedimentology. *Acta Sedimentologica Sinica*, 15(4): 67–71. (in Chinese)
- Pennington W, Cambray R S, 1973. Observations on lake sediments using fallout  $^{137}\text{Cs}$  as a trace. *Nature*, 242: 324–326.
- Perianez R, 2008. A modeling study on  $^{137}\text{Cs}$  and  $^{239,240}\text{Pu}$  behaviour in the Alboran Sea, Western Mediterranean. *Journal of Environmental Radioactivity*, 99: 694–715.
- Ren Mei'e, 1986. China Comprehensive Investigations of the Coastal Zone and Tidal Land Resources. Beijing: Ocean Press, 36–180. (in Chinese)
- Shigeru M, Futoshi N, Tohru A, 2006. Using dendrogeomorphology and  $^{137}\text{Cs}$  and  $^{210}\text{Pb}$  radiochronology to estimate recent changes in sedimentation rates in Kushiro Mire, northern Japan, resulting from land use change and river channelization. *Catena*, 68: 25–40.
- Sun Youbin, Gao Shu, Li Jun, 2003. Primary analysis on the sensitive grain-size of terrigenous sediment to environments in marginal sea. *Chinese Science Bulletin*, 48(1): 83–86. (in Chinese)
- Thorbjorn J A, Ole A M, Annette L M *et al.*, 2000. Deposition and mixing depths on some European intertidal mudflats based on  $^{210}\text{Pb}$  and  $^{137}\text{Cs}$  activities. *Continental Shelf Research*, 20: 1569–1591.
- Wan Guojiang, 1995. Progresses on  $^{137}\text{Cs}$  and  $^{210}\text{Pb}_{\text{ex}}$  dating of lakes sediments. *Advance in Earth Sciences*, 10(2): 188–192. (in Chinese)
- Wang Aijun, Gao Shu, Jia Jianjun *et al.*, 2005. Contemporary sedimentation rates on salt marshes at Wanggang, Jiangsu, China. *Acta Geographica Sinica*, 60(1): 61–70. (in Chinese)
- Wang Aijun, Gao Shu, Jia Jianjun, 2006. Impact of the cord-grass *Spartina alterniflora* on sedimentary and morphological evolution of tidal salt marshes on the Jiangsu coast, China. *Acta Oceanologica Sinica*, 25(4): 32–42.
- Wang Aijun, Wang Yaping, Yang Yang, 2004. Surface sediment characteristics and transport trends on the Wanggang intertidal flat, Jiangsu Province. *Acta Sedimentologica Sinica*, 22(1): 124–129. (in Chinese)
- Wang L, Sarnthein M, Erlenkeuser H *et al.*, 1999. East Asian monsoon climate during the Late Pleistocene: High resolution sediment records from the South China Sea. *Marine Geology*, 156: 245–284.
- Wang Ying, Zhu Dakui, 1990. Tidal flats of China. *Quaternary Sciences*, 4: 291–299. (in Chinese)
- Wu Xiaogen, Wang Aijun, 2005. Impacts of human beings activities on north Jiangsu tidal flat. *Scientia Geographica Sinica*, 25(5): 614–620. (in Chinese)
- Xia Xiaoming, Yang Hui, Li Yan *et al.*, 2004. Modern sedimentation rates in the contiguous sea area of Changjiang Estuary and Hangzhou Bay. *Acta Sedimentologica Sinica*, 22(1): 130–135. (in Chinese)
- Yang Guishan, 2002. Coastal Environmental Change and Its Regional Responses in China. Beijing: Higher Education Press, 144–149. (in Chinese)
- Yang Guishan, Shi Yafeng, Ji Zixiu, 2002. The ecological response of typical mud flat to sea level change in Jiangsu coastal plain. *Acta Geographica Sinica*, 57(1): 76–84. (in Chinese)
- Zhang Renshun, 1986. The characteristics of tidal currents and the sedimentation progress of suspended particles of tidal mud flat in Jiangsu Province. *Oceanaologia et Limnologia Sinica*, 17(3): 235–245. (in Chinese)
- Zhang Renshun, Lu Liyun, Wang Yanhong, 2002. The mechanism and trend of coastal erosion of Jiangsu Province in China. *Geographical Research*, 21(4): 469–478. (in Chinese)
- Zhang Yan, Peng Buzuo, Chen Jie *et al.*, 2005. Evaluation of sediment accumulation in Dianchi Lake using  $^{137}\text{Cs}$  dating. *Acta Geographica Sinica*, 60(1): 71–78. (in Chinese)
- Zhu Dakui, Ke Xiankun, Gao Su, 1986. Tidal flat sedimentation of Jiangsu coast. *Journal of Oceanography of Huanghai & Bohai Seas*, 4(3): 19–27. (in Chinese)